CHAPTER 10

IMAGING SPECTROSCOPY APPLICATIONS IN FOOD QUALITY MEASUREMENTS

JESPER BRØNDUM[$#], LARS MUNCK[$*] AND ERLING LARSEN[¤]

TO BE SUBMITTED

$ Food Technology, Dept. of Dairy and Food Science, Royal Veterinary and Agricultural University, Rolighedsvej 30, 1958 Frederiksberg, Denmark

\# SFK Technology A/S, Transformervej 9, 2730 Herlev, Denmark

¤ Department of Fishstudies, Research Laboratory, Danish Technical University, 2800 Lyngby, Denmark

* Author for correspondence.

ABSTRACT

The design and functionality of an imaging spectrograph creating spectra and images for food quality measurements is outlined. The system is constructed using a very sensitive CCD array, a rotating grating holder, and a UV objective. Using binning of the CCD array, up to 330 local spectra in the UV/VIS/NIR range can be collected from an area of up to 22×70mm with the UV objective available. The performance of the imaging spectrograph was compared to a laboratory spectrofluorometer in predicting ash and colour in wheat flour mill streams. The imaging spectrograph was tested in experiment following post-mortem changes in fish meat. Based on binning data an algorithm for spectral homogeneity was created and compare with image analysis from the same imaging spectrograph in studying fish and meat homogeneity. It was concluded that the imaging spectrograph was able to give combined access to both spectral and structural data in seconds making it an interesting sensor for further development of food quality applications.

INTRODUCTION

On-line measurement of food attributes is increasingly important in food processing due to the demand for defined product quality and process control due to regulations and competition. Thus the development of fast non-destructive "on-line", "at-line" screening analyses have become important in the food processing industry. Development of sensors for process and quality control has been identified, as a critical area in food engineering research needs (Jenks *et al.* 1996; Caro, 1991) (Hui, 1996; Dziezak, 1986; Giese, 1993). The major obstacles for the implementation of on-line measuring methods have been the complex and variable nature of food and the lack of availability of adequate monitoring and sensing methods.

Sampling methodologies in space and time are critical with respect to qualitative and quantitative assessment of inhomogeneous food products. Sampling schemes involving grinding, mixing, homogenisation and extraction in order to obtain a more selective analytical response suffer inherently from the drawbacks that these methods are destructive and not readily applicable in a high-throughput industrial production area.

Ongoing developments in the fields of computer vision of foods (Gunasekaran, 1996), on-line spectroscopy (Swatland, 1995), and multivariate data analysis in industrial applications (Munck *et al.* 1998), may be integrated to a system that facilitate the development of on-line food assessment systems. An ideal on-line quality-measuring device e.g. based on spectroscopy will be able to measure non destructively a great number of unselective data points from which relevant quality parameters can be extracted by chemometric software through calibration to classical destructive analyses.

In traditional imaging monochrome images are acquired of the object. In studies where a more extensive wavelength information is required, a colour vision system with a RGB CCD array is most often used. In more advanced studies, where the three colour ranges do not meet the requirements, a filter approach is often used. One commercial example of this is the Dipix fluorescence microscope for flour analyses (Dipix Technologies, Inc., Ottawa, Ontario, Canada), where a monochrome camera is combined with a set of filters for controlling both the illumination and the acquisition wavelength inspired by the initial work by (Jensen *et al.* 1982). The drawbacks of the multichannel techniques are clearly that the technique is either slow (the filter approach) and/or with a low and non flexible spectral resolution (the colour CCD).

Spectroscopy introduces the possibility of measuring with a very high spectral resolution. Typically every nanometer is measured in commercial laboratory spectrometers. Examples are the Perkin Elmer LS-50 spectrofluorometer (Buckinghamshire, UK) which are widely used in laboratory systems, and the NIR Probe FQM (Danish Meat research Inst., Roskilde, Denmark). All these techniques do however, suffer from the problems with measuring a representative area of the object. An obvious example is the PE LS-50, which measure a surface of 1×9 mm of the sample. Obviously this affects the measurement representation when measuring non-homogenous food products as e.g. meat with laboratory equipment.

In order to meet the requirements of a representative on-line assessment of food quality characteristics this study combine traditional imaging and spectroscopic techniques by introducing a novel technique - the CCD imaging spectrograph. Thereby both spatial and spectral information is obtained on reasonable large sample areas in order to obtain representation of inhomogeneous food products.

The technique is demonstrated with experiments involving combined time-resolved image analysis, reflectance and fluorescence spectroscopy and evaluated by multivariate data analysis in theoretical test situations and in food quality inspection of flour refinement, post mortem fish meat changes and pork meat homogeneity.

MATERIAL AND METHODS

PRESENTATION OF THE IMAGING CCD SPECTROGRAPH SYSTEM

The ST-138 system from Princeton Instruments Inc. (Trenton, NJ) is in combination with the Spectra Pro-150 spectrograph from Acton Research Corporation (Acton, MA) a flexible multi-use imaging and spectroscopic instrument. The system is based on a software controlled charge coupled device (CCD), which samples spectral information from a UV objective through grating diffraction light dispersion or alternatively images through a mirror (see Figure 1).

The CCD based spectrograph system consists of a set of modules, of which the CCD camera, the movable turret containing gratings and/or mirror, the slit width adjustment, the UV objective and the personal computer (PC) are the most important. The combination of these modules gives the possibility of measuring ultra violet (UV) visual (VIS) and near infrared (NIR) spectra of large sample areas. It is possible to combine pixel arrays through binning to divide the region of inspection into several spatial regions by software control of the CCD array. Thereby the data acquisition combines local and global imaging and spectral information from the surface under inspection.

Figure 1. Schematic overview of the imaging spectrograph system. The measured spectra are projected from the objective to the CCD array via the grating. By rotating the grating holder, the mirror can be used instead, and the CCD can be used as a traditional camera system.

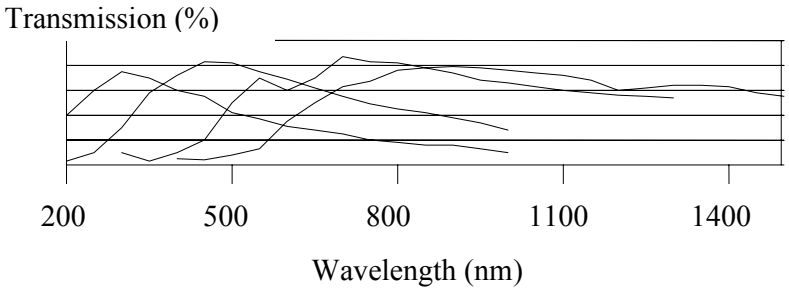

Figure 2. Wavelength characteristics for the four gratings.

Figure 3. Five colours measured spectroscopic. Five colours (violet, blue, green, yellow, red) are measured with the CCD array. Using binning, 10 spectra are collected from the colour plot (two from each colour). The reflectance spectra from bin 1 and bin 10 are shown to the right. To the left a mesh plot of the entire 10 spectra are shown.

The main modules of the spectrometer are illustrated in Figure 1. The remote sensing system is capable of measuring objects at a distance of approximately 1 meter with the Nikon 105mm UV objective giving a maximum measurement area of 22×70mm. The incoming light is either reflected to the CCD array using the mirror if images are acquired or to diffraction by the grating onto the CCD array if spectra are acquired. By rotating the turret between the mirror and the grating position enable acquisition of both images and spectra from the surface. Alternatively, for faster image acquisition in practical measurements the zero order refraction of the grating can be used. Thereby the time consuming turret rotation between the mirror and the grating is saved, but on the cost of a slightly poorer image quality at the border of the image.

Four gratings are available and can be combined (two can be contained in the turret). This enables spectroscopic measurements in the spectral range from 200-1100 nm as illustrated in the wavelength characteristics of the gratings shown in Figure 2. Our CCD array is liquid nitrogen cooled in order to obtain maximum sensitivity (the dark current charge is less than 0.4 electrons/hour). UV coating of the CCD array ensures that the UV sensitivity of the gratings is utilised by the spectrometer. The CCD array is back illuminated and a quantum efficiency of about 80 % ensures a minimal signal loss due to absorption.

The size of the rectangular CCD array is 1100×330 pixels (Figure 3). This is chosen as opposed to a quadratic array in order to accommodate large range spectra with a high resolution. The horizontal (1100) dimension is used for the spectral dimension and the vertical dimension is used for the spatial resolution. For each of the 330 spatial lines a spectrum of 1100 wavelength measurements can be read. By combining the horizontal rows of the CCD array into spatial regions with binning, a lower number of spectra are acquired. Binning has the advantage of reducing the integration time and enabling the acquisition of signals with low intensity. As an example, binning the CCD array into 10 regions of 33 pixel rows each, 10 local spectra with 1100 spectral points are achieved in one instant acquisition.

IMAGE ANALYSIS

The images acquired from the CCD imaging spectrograph in the traditional camera mode are processed with digital image analysis. The purpose of the image analysis is to extract information from the object by extraction of image features. Image features are often separated into two main groups: structural and textural. Where the former group of features describe the shape of the object, the latter describe the pattern of the surface of the object. In this work, all attention is focused on textural features due to the nature of the food products being analysed in this study. Four groups of features are used: 1) statistical features, 2) co-occurrence matrix features and 3) angular moment transformation features.

Statistical features. The statistical features describe the surface texture of the object by inspecting the intensity mean, variation, root mean square, population skewness, and population kurtosis. A second statistical feature description is performed on the images after a fractal transformation is applied. The fractal transformation estimates the fractal dimension in a region in the image surrounding each pixel. The fractal dimension is estimated using the Hurst coefficient (Russ, 1994) and (Mandelbrot *et al.* 1984). The fractal transformation results in a new image with the textural regions highlighted. The statistical features described above are extracted on the transformed image. Hence, up to totally 10 statistical features are used.

Co-occurrence matrix features. The intensity moment features are based upon calculation of the co-occurency matrix (COM). The COM displays the intensity difference between the neighbouring pixels. Thus, a COM with near-zero members reveal a low textured region, whereas high values in the matrix can be interpreted as the region being highly textured. Nine features are output from the COM: the variance, the 3^{rd}, 5^{th}, 6^{th} and 7^{th} moment, the maximum index, the entropy, and the sum of squares. (Conradsen, 1989) and (Haralick *et al.* 1973).

Angle moment transformation. The angular moment transformation was originally proposed for geological studies by (Andrle, 1994) and later adapted to multivariate image analysis by (Esbensen *et al.* 1996). The signal is transformed from the image domain to a scale domain given by the Euclidean distance between the intensities of neighbouring pixels. The intensity in the scale domain is given by the angle between the two intensity vectors intersecting two neighbouring points at a specific distance. The calculated angle is averaged over numerous pixels (we have used 300) and output as a function of the scale. We have used a scale varying from 1 to 100 resulting in 100 features. Extraction of all image features has been performed in software developed in the Khoros 2.2 software (Khoral Res.Corporation, NM).

MULTIVARIATE DATA ANALYSIS

The spectroscopic methods generate large data amounts. Instead of selecting a single representative wavelength from the spectra it is advantageous to use all the information present in the full spectrum. This leads to the use of multivariate data analysis as represented by the field of chemometrics in food quality inspection. The two primary chemometric tools are the principal component analysis (PCA) mainly for interpretative purpose, and partial least squares regression (PLS) for data regression studies. *PCA* is a method for decomposing a set of multivariate measurements into a smaller number of variables with a minimal loss of information. The decomposition results in a score matrix and a loading matrix, where the score values describe the samples in the new dimensions, and the loadings describe the common structure in the original samples. For more information about PCA, see sources like (Martens *et al.* 1993), (Wold *et al.* 1987), (Esbensen *et al.* 1994). PLS is in chemometrics often used to correlate fast acquired spectroscopic data with slow or expensive chemical or sensory data. The method work similar to PCA by decomposing the original samples into a new set of scores and latent variables (similar to the loadings for the PCA). The decomposed data are then used for regression between the score values for the chemical/reference variable. PLS is more extensively described in (Martens *et al.* 1993), and (Esbensen *et al.* 1994), (Bro, 1995). Multivariate analysis was carried out with program suites: Unscrambler 7.0 (CAMO A/S, Trondheim, Norway) and MATLAB 5.2 (The Mathworks Inc., MA).

HOMOGENEITY INDEX

To combine the imaging and the spectroscopic functionality of the spectrograph, an index of homogeneity with the purpose of describing the surface structure is developed. The homogeneity index (HI) can be obtained from the acquired data due to the binning technique of the CCD array, which enable spectra from local domains of the image to be studied. With HI calculated from the local spectra, the imaging spectroscopic system could be used to evaluate the homogeneity of the sample based on information from large spectral regions. In traditional spectroscopy, a mean spectrum is obtained from the sample, with no spatial and homogeneity information. In multichannel imaging, optical filters are used to obtain more and less monochromatic images at defined wavelength channels from the sample. By acquiring an image at each wavelength of interest, a high spatial resolution is gained. This is, however, on the cost of a much lower spectral resolution due to the usually wide transmission range of the optical filters. Furthermore, if a large number of spectral points are of interest, the data amount and the acquisition time are increased significantly by the rising number of exposures. Hence, studying homogeneity by binning the CCD array is a new approach to combine high spectral and spatial resolution with a very fast data acquisition.

HI is calculated from the variation of the spectral points over the spatial position. The data is interpreted as a one-dimensional image with a spectrum in each bin. The spectral information is transformed into a single statistic measure for each bin. The HI is then calculated by performing traditional image analysis on the one-dimensional image containing the statistic information about the spectra in each bin.

Notation. Let M denote the number of bins (spectral regions) and *N* denote the number of spectral points for each bin. *m* and *n* are the corresponding indices for these two variables. Let $x_{m,n}$ denote the pixel intensity for the m'th and the n'th index. $P(x_{m,n})$ denote the normalised probability of the intensity of $x_{m,n}$.

The first step in the algorithm of the *HI* is calculation of the pixel-wise information from the spectral information. Two approaches to this are tested 1) the variance and 2) the entropy, as described in equation 1 and 2.

$$\mathrm{var}_m = \frac{1}{N}\sum_{m=0}^{N}(x_{m,n} - \bar{x})^2 \qquad (1)$$

$$entropy_m = \frac{1}{N}\sum_{n=1}^{N} - P(x_{m,n})\log(P(x_{m,n})) \qquad (2)$$

For calculating the entropy, the probability function P is estimated with a histogram function with 25 bins for each spectrum individually.

From equation 1 and 2, the HI can now be calculated using one of two approaches 1) mean value and 2) median value. For equation 1, this leads to equation 3 and 4, and similar equations can be developed for equation 2.

$$HI_{mean} = \frac{1}{M}\sum_{m=1}^{M} var_m \qquad (3)$$

$$HI_{median} = median(\underline{\text{var}}) \qquad (4)$$

where $\underline{\text{var}}$ describes a vector with all M variances.

EXPERIMENTAL DESIGN

System Pretests. To demonstrate the functionality of the spectroscopic system a set of pretests are conducted. The first pretest is designed for mapping the slit width to the resulting size of the vertical field of view at a given distance (see Table 1 and Figure 4). The objective is focused on a squared paper at distances of 85cm and 100cm. The slit width is adjusted from the minimal size (0.0mm) to the maximum (3.0mm) and the horizontal field of view is measured.

The second pretest deals with the effect on the spectra by adjusting the slit width. The reflectance spectra of an Oriel Hg (A) lamp (Oriel, Stratford, CT, USA) with extensive peaks at specific wavelengths are measured with three different slit widths of 0.1mm, 0.5 mm and 2.0mm (see Table 1 and Figure 5).

The third test deals with binning the CCD array. Reflectance spectra of simple colour plot containing 5 colours are measured (Figure 3). The number of bins is adjusted from 20 to 82, whereby the number of spectra representing each of the five colours is reduced from 16 to 4. PCA is performed on the spectra and the grouping of the five colour regions are observed (see Table 1 and Figure 6). During all pretests, the CCD sensor is kept at -70°C.

Figure 4. The slit width versus the horizontal field of view. The top figure shows the focal distance 1000mm where a maximum field of view of 22mm. The bottom figure shows the focal distance 850mm where a maximum field of view of 22mm.

Figure 5. The reflectance spectra of a Hg calibration lamp. a) With a slit width of 0.1mm. b) With a slit width of 0.5mm. c) With a slit width of 1.0mm.

Table 1. Acquisition parameters for the spectral measurements on the imaging spectrograph.

	Spectroscopic Mode	Integration Time	No. Bins	Field of View (Measured area)	Illumination*
Pretest 1 (Field of view)	Reflectance	500ms	1	0×70mm to 22×70mm	Visual range
Pretest 2 (Spectral Resolution)	Reflectance	500ms	1	2×70mm, 6×70mm, 11×70mm	Visual range
Pretest 3 (Binning)	Reflectance	500ms	20, 82	10×70mm	Visual range
Application 1 (Flour)	Fluorescence	1000ms	6	10×70mm	Ex.:280,340, 380,460,480nm
Application 2 (Fish)	Reflectance	500ms	6	10×70mm	Visual range
	Fluorescence 1	1000ms	6	10×70mm	Ex.: 290nm
	Fluorescence 2	1000ms	6	10×70mm	Ex.: 380nm
Application 3 (Porcine meat)	Reflectance	500ms	10, 41, 110	20×70mm	UV range

* All reflectance measurements are made with a Light Board including both a UV range (200-400nm) and a Visual range (400-700nm). All fluorescence measurements are made with an Uhl monochromator.

Application 1: Comparative Instrument Test - Spectroscopic Measurements of Wheat Flour Refinement. This experiment is done in order to compare the performance of the imaging spectrograph with a laboratory spectrofluorometer and a scanning low magnification florescence imaging microscope. Fluorescence measurements are made on 36 wheat flours streams collected in a Danish wheat mill. For comparison, the samples were also measured with the Perkin Elmer LS-50 spectrofluorometer and the Dipix I440 fluorescence microscope (Maztech MicroVision Ltd., Ottawa, Ontario, Canada). Using a monochromator the excitation wavelengths: 280nm, 340nm, 380nm, 460nm and 480nm are used and the total emission spectra are acquired (see Table 1). Furthermore reference information of the flour refinement is made with colour measurements with an Agtron M-45 and laboratory ash, fibre and starch measurements. Attempts to predict the reference information are made from the spectra made with all spectroscopic systems. All measurements are carried out at ambient temperature and with the CCD sensor cooled to -70°C.

Application 2: Imaging Spectroscopy Detection of Fish Ageing. Fresh (48 hours) iced salmon (class A, 5-10 kg) is filleted and minced and frozen in liquid nitrogen and kept in a freezer until gentle thawing in a refrigerator, immediately preceding the experiments. Rainbow trouts (5 kg) are caught 90 minutes before the start of the experiments. The samples were measured over a period of 8 hours at intervals of 30 minutes. Both visual images and reflectance (using a light board for illumination), and fluorescence spectra with excitation of 290nm and 380nm (using an Uhl monochromator for illumination) were measured (see Table 1). All measurements are carried out at ambient room temperature and with the CCD sensor cooled to -70°C.

Application 3: Homogeneity Study of Pork Meat Related to Marbling. Six samples from five porcine muscles: longissimus dorsi (ld_1 and ld_2), lumber vertebra (lv), semitendinosous (st), semimembranosous (sm), and belly (be), are purchased approximately 24 hours post mortem and have not been frozen. The samples are graded from 'practically devoid' to heavily marbled' according to the NPPC marbling standards (NPPC, 1991) by a trained meat inspector. Reflectance spectra from the samples are measured with UV light (max peak at 366 nm) from a light board. The spectra are collected with three different numbers of bins: 10, 42 and 110 (see Table 1). HI is calculated with all four combinations of entropy and sd, and mean and median. The four HI's for each of three bin options are compared to the entropy and the miximum index of the co-occurrence image texture features. All measurements at ambient room temperature and with the CCD sensor cooled to -70°C.

RESULTS AND DISCUSSION

SYSTEM PRETESTS

The objective of the first pretest is to define the effect of the slit width on the size of the inspected region. Figure 4 shows the measured horizontal field of view when adjusting the slit width from 0.0mm to 3.0mm. The field of view (FOV) is measured for two different lens to object, 1000mm and 850mm. A nearly linear relation between FOV and the slit width is observed, and maxima of 22mm and to 20mm at 3.0mm slit width are observed respectively for the two distances. Larger fields of view can be measured by the imaging spectrograph if a suitable UV-objective is available.

The second pretest demonstrates the effect of the slit width on the spectral resolution. Reflectance spectra of an Oriel Hg calibration lamp are recorded as the slit width is adjusted. The spectra of the three slit widths (0.1mm, 0.5mm and 2.0mm) are shown in Figure 4. It is observed that increasing the slit width results in decreasing spectral resolution but gives a higher intensity level. The increasing signal intensity follows from the larger area measured. The less well defined peaks are due to the grating diffraction. It is our experience that the spectra measured at even the highest slit width give the largest field of inspection is highly reproducible and may be used to extract empirically validated spectral information from the samples by multivariate data analysis.

The effect of binning is demonstrated and better understood with the third pretest. The colour plot measured containing the 5 colours red, green, yellow, violet, blue illustrated in Figure 3 is measured with a varying number of bins. The spectra shown in Figure 3 are acquired with 10 bins and the mesh plot in Figure 3 contain two measurements from each colour. By increasing the number of bins from 10 to 20 and 82 we, also increase the number of spectra representing each of the five colours to 4 and 16. Two interesting observations are made from the spectra (data not shown). Firstly, the intensity level decreases as the number of bins is increased because the integration area is decreased. Secondly, the noise level is raised when the number of bins is increased. Figure 6 shows the scatterplot from PCA's of the spectra from the two experiments with 20 (Figure 6a) and 82 bins (Figure 6a) respectively. In both score plots the spectra tend to fall into 5 classes, one for each colour. As observed, some of the spectra are observed in-between two classes as e.g. number 9 in Figure 6a and number 34 in Figure 6b. This effect is caused by the fact that the binned regions at the intersection between two colours actually will contain both colours. Furthermore, small errors may be due the fact that the printed colours on the paper is slightly overlapping due to a printer of limited quality and because the plot may not be totally aligned with the slit opening.

Figure 6. PCA scoreplot for the reflectance spectra measured on a colour plot with five colours. Top: Using 20 bins. Below: Using 82 bins. In both plots, the five groups of points are ordered from low left corner to the top right corner as follows: Red, Yellow, Green, Violet , Blue.

Apart from full area spectroscopy and spatial binning to study local areas in the field of view, it is also possible to use the system for standard imaging. By using full slit opening and reflection (as opposed to diffraction) from the grating an image of approximately 60×60mm at a distance of 1m from the objective is acquired. The standard imaging mode is further explained in the food applications.

The results of the pretests are used to design an optimal setup in food measurements. Optimising the slit width is a compromise between signal intensity level and sample representation versus spectral resolution. Due to the cooling system in the CCD array, the integration time can be increased to compensate for low intensity levels. The signal intensity is therefore not essential when choosing the slit width unless a very fast data acquisition is necessary. Most often the most significant question is whether to optimise for measurement area or for spectral resolution. When working with food products, it is often most advantageous to acquire signals with a wide slit opening ensuring a large area of inspection due to the inhomogeneity of the media.

APPLICATION 1: FLUORESCENCE MEASUREMENTS OF WHEAT FLOUR REFINEMENT

The imaging spectrograph is applied to the flour refinement application to demonstrate the remote sensing efficiency in spectroscopic measurements and compare it to a laboratory spectrofluorometer and a scanning fluorescence microscope. The botanical components (pericarp, aleurone and aleurone) can be measured with autofluorescence as described by (Jensen *et al.* 1982) and (Munck, 1989). The different excitation wavelengths produce emisson spectra revealing the botanical components endosperm (at 280 nm), aleurone (at 340, 380 nm), and aleurone (at 460, 480 nm). The chemical analyses starch, ash and fibre are indicative for endosperm, aleurone, and pericarp respectively. The pericarp (fibre) component is highly coloured. 43 very different wheat milling stream samples from a diagram of an industrial wheat mill are measured. The range of the reference characteristics were as follows: ash (0.34 - 1.86%), colour (42 - 79 units), crude fibre (1.82 - 15.89%, starch (61.7 - 80.3%) and gluten (0 - 36.6%).

The spectral acquisitions made on the CCD imaging spectrograph are compared to measurements made on the Perkin Elmer LS-50 and the Dipix. The data are used in a PLS calibration validated with full cross (leave one out) validation to flour colour, ash, fibre and starch. Results of the PLS predictions made of the reference are given in Table 2.

Table 2. Standard error of prediction (SEP) and correlation (r) of the colour, ash, fibre and starch values of the wheat flours with the spectroscopic systems.

	Colour		Ash		Fibre		Starch	
Instrument	r	SEP	r	SEP	r	SEP	r	SEP
Imaging Spectrograph	0.96	2.43	0.92	0.203	0.78	0.38	0.87	3.18
DIPIX	0.94	3.10	0.92	0.200	0.89	1.04	0.80	3.08
PE LS-50	0.96	2.51	0.92	0.206	0.85	1.16	0.84	2.80

It can be concluded from the results in Table 2 that all the fluorescence methods were equal in their ability to predict the most important analyses of ash (r=0.91-92) and colour (r=0.94-96), while correlations to fibre (r=0.78-0.89) and starch (r=0.80-0.87) were lower. It should be reminded that non-homogeneities and the representativity of sampling is highly variable between these instruments given the measurement area of 1 x 9 mm for the spectrofluorimeter, 22×70 mm for the imaging spectrofluorimeter and 50 x 100 mm for the fluorescence DIPIX microscopes. Usable excitation and emission wavelengths also varied among the instruments. There were no significant correlation to gluten.

APPLICATION 2: IMAGING SPECTROSCOPY DETECTION OF FISH AGEING

Fish ageing. The efficiency of the Princeton Instrument for analysing inhomogeneous media is demonstrated on a fish ageing study on salmon mince and trout muscle and skin. During a period of 8 hours fluorescence, reflectance and imaging data were acquired in intervals of 30 minutes to follow spectrally the muscle development during ageing. Figure 7 shows the spectroscopic data for the minced salmon and Figure 7 shows the images from the three sample types.

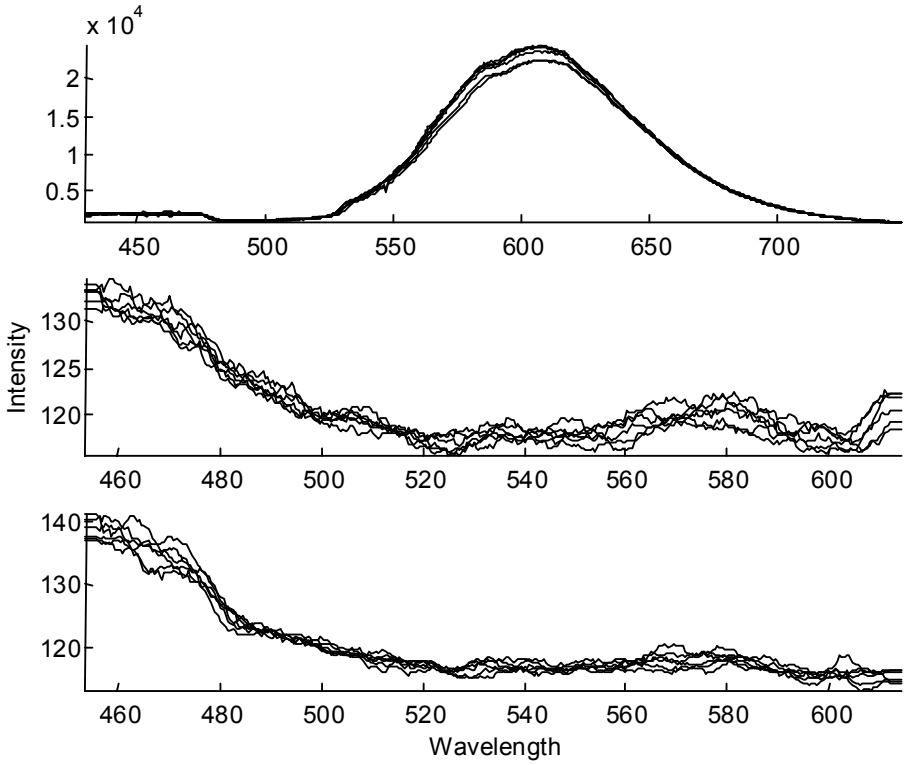

Figure 7. Six spectra of the minced Salmon. Top: Reflectance. Middle: Fluorescence with excitation 410nm. Bottom: Fluorescence with excitation 410nm.

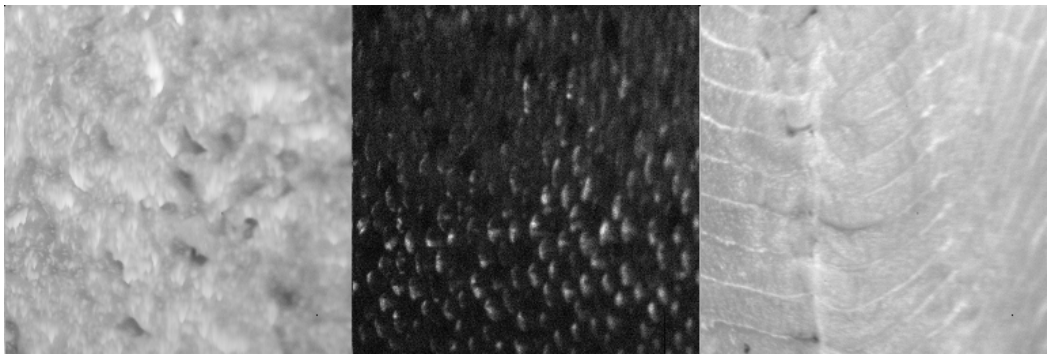

Figure 8. Images of a) Minced Salmon, b) Trout skin, and c) Trout fillet.

To investigate whether the spectra obtained from the imaging spectrograph show changes which are related to the time post-mortem of a minced salmon sample, a principal component analysis was carried out on the fluorescence spectra. A scoreplot for fluorescence spectra from trout fillet is displayed in Figure 9 showing a characteristic horseshoe pattern starting with the 30 min. old sample to the right and ending with the 510 min. old sample to the left. There is a drastic jump from 120 to 150 min., which coincides with rigor. In the onstart, chemical processes such as the decay of the fluorescent co-enzyme NADH dominate (this was studied in a separate student project, but not reported here), while at the end of the eight-hour storage at room temperature bacteriological effects should overlayer those of autolysis.

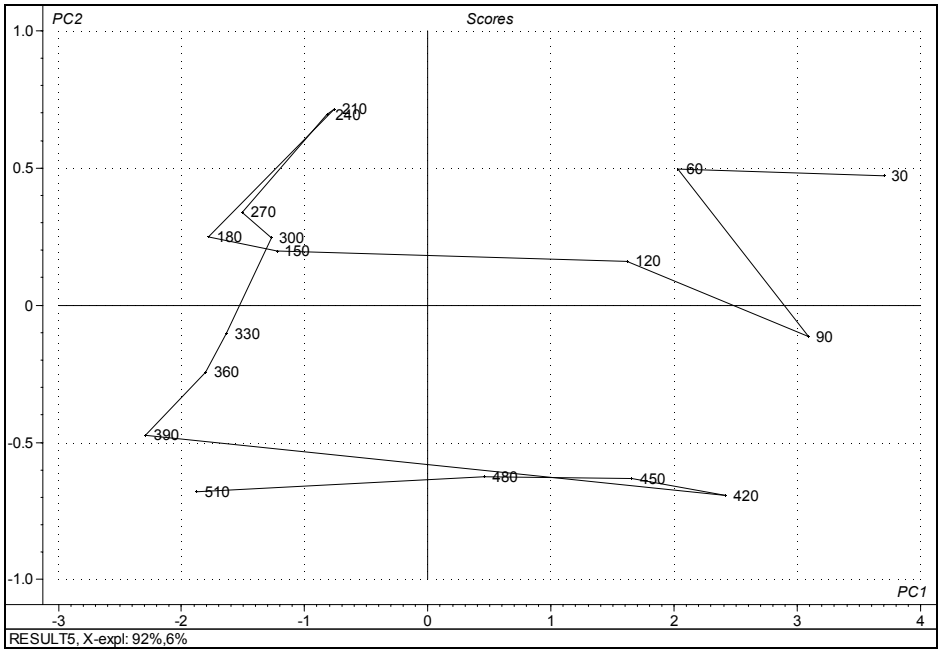

Figure 9. PCA scoreplot of the fluorescence spectra from trout meat monitoring experiment. Figures are storage time at room temperature in minutes.

Using the time development post-mortem as a reference parameter, the spectroscopic data was calibrated to predict the time development as shown in Table 3. These results indicate that a fast CCD-camera is capable of recording early post-mortem changes in fish. These changes in the muscle food during the measurement periods might relate to the rapid biological processes caused by the oxygen deprivation of the muscle tissue post-mortem and changes in fluorescent compounds of physiological importance, such as nicotine adenine dinucleotide hydride (NADH) (Jenks *et al.* 1996). Spectral changes are also likely to occur due to changes in the reflectance scattering because of the muscle contraction. An accurate prediction of the post-mortem time of a muscle food material will be useful in an industrial environment, if a generally valid calibration model could be established for many individuals from the same meat animal species. However, as in all exploratory work involving "reversed engineering", an enormous amount of work remains in verifying and calibrating the underlying reactions and in making the analysis generally applicable by a data bank of artificial intelligence. The idea of research given by this experiment could, however, be economically implemented by joining existing research and complementing with the spectrofluorometric and chemometric options, if spectrofluorimeters with greater measurement area could be constructed. Our further research efforts are directed towards remote spectral screening techniques for predicting muscle material freshness calibrated to changes in chemical composition and microbial and sensory quality.

The homogeneity of the minced meat is investigated with the HI. The HI is calculated from the 6 different reflectance spectra using entropy and variance, and mean and median. The correlation between the two co-occurrence texture image features was highest for the HI combining variance and mean with correlation of 0.74 and 0.71 to the image features. The success of the HI suffers largely from the low number of bins in this trial. The feasability of the HI is further discussed in the next section.

Table 3. Prediction errors (in minutes) and correlation coefficients r based on the spectral and the imaging data over a period of 0-8 hours post-mortem. N/A denotes not applicable.

	Image Features		Reflection spectroscopy (visual range)		Fluorescence spectroscopy (ex. 290nm)		Fluorescence spectroscopy (ex. 380nm)	
	SEP	r	SEP	r	SEP	r	SEP	r
Minced Salmon	92	0.80	36	0.96	71	0.81	53	0.92
Trout Fillet	76	0.86	28	0.97	60	0.93	35	0.95
Trout Skin	92	0.80	51	0.94	N/A	N/A	N/A	N/A

APPLICATION 3: HOMOGENEITY STUDY OF PORK MEAT RELATED TO MARBLING

The 6 porcine samples are shown in Figure 10 ordered by the degree of marbling. The marbling occurs due to the intramuscular fat, which is known to be highly reflecting in UV light (Jensen *et al.* 1989). The samples are therefore measured with UV reflectance (see Table 1) with a varying number of bins. For comparison with traditional imaging techniques, the samples are also measured under visual illumination with normal imaging mode. The spectroscopic and image measurements are compared to a visual classification of the degree of marbling and a sorting of the samples due to the homogeneity performed by a trained meat inspector.

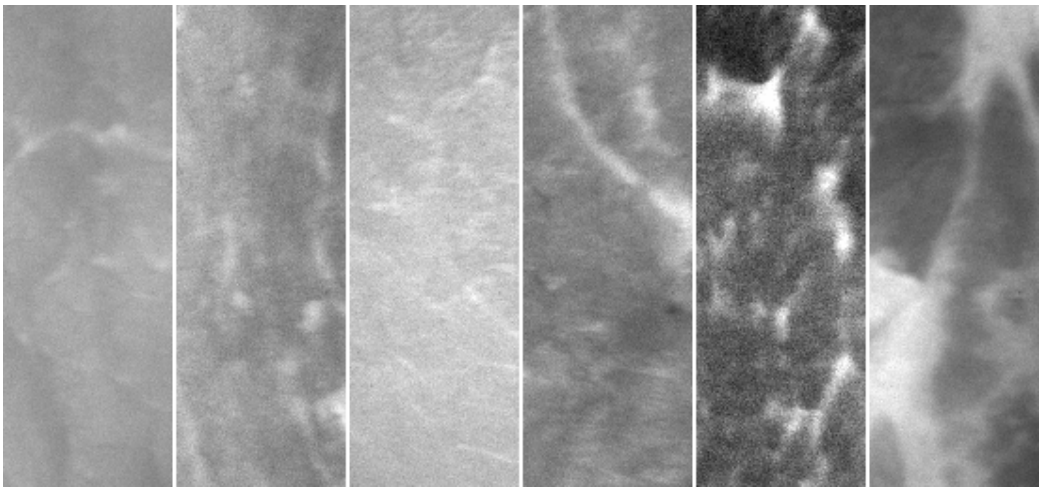

Figure 9. Images of the six pork samples ordered by homogeneity. a) ld_1, b) ld_2, c) lv, d) st, e) sm, and f) be.

The homogeneity indices are calculated for the three different numbers of bins 10, 41, and 110, using both variance and entropy, and mean and median as explained in the theoretical section. This results in a total of 12 HI values.

The visual scores following the NPPC standards, correlate with r=0.98 with the order index, as shown in Table 4. The correlation between the visual scores and the 12 HI values are calculated. The highest correlation values between the visual scores and the HI were r=0.80, r=0.92, and r=0.94 for 10, 42, and 110 bins respectively. The results are shown in Table 4, which is a cross correlation table presenting the correlation between the homogeneity order, the visual score, the HI_{10}, HI_{42}, HI_{110}, (HI_{10} indicates the HI calculated for 10 bins, etc.) and the image texture features COM_1, and COM_2.

As noted in the footer of the table, the optimal HI for the three numbers of bins were not obtained with the same statistic measures. Where HI_{10} and HI_{110} were optimal by combining the variance and the mean, the combination of the entropy and the mean was optimal for the HI_{42}. This indicates that the optimal HI may not be deducted, and more improvement may be expected.

Table 4. Cross correlation table between the homogeneity order, the visual marbling score, the three Homogeneity Indices, and the two Co-occurrence Matrix texture features. Each cell in the table shows the correlation between the features given in the row and the column headers.

	Order	Visual	HI_{10}*	HI_{42}**	HI_{110}***	COM_1¤	COM_2¤¤
Order	1.00	0.98	0.77	0.93	0.90	0.78	0.93
Visual		1.00	0.82	0.92	0.94	0.87	0.87
HI_{10}*			1.00	0.85	0.95	0.65	0.65
HI_{42}**				1.00	0.92	0.78	0.80
HI_{110}***					1.00	0.79	0.74
COM_1¤						1.00	0.85
COM_2¤¤							1.00

* HI_{10} is calculated with 10 bins, using variance and mean.

** HI_{42} is calculated with 42 bins, using entropy and mean.

*** HI_{110} is calculated with 110 bins, using variance and mean.

¤ COM_1 is the maximum index of the co-occurrence matrix.

¤¤ COM_2 is the entropy of the co-occurrence matrix.

The improving performance of the HI with the increasing numbers of bins is as expected. The improvement from 42 to 110 is however very limited (0.92 to 0.94 relative to the visual scores). Actually inspecting the image texture features and the order of homogeneity, indicate the difference between HI_{42} and HI_{110} to be non-significant. This is due to two causes. Firstly, the homogeneity of these specific samples is well described by the 42 different regions. Secondly, the increased number of bins cause the noise level in the spectra to increase. Thus, measuring the homogeneity of a sample using imaging spectroscopy is a compromise between the number of regions and the spectral noise level.

Comparing the results achieved for the HI and the image texture features show a better performance of the HI measures. This supports the hypothesis that an increased wavelength information obtained in the UV area is superior to the image greyscale intensities in the visual range. In the current application the fat reflection response is surely different in the UV wavelength range than in the visual range. The difference in the illumination source is also believed to be the reason for the limited correlation values observed between the HI and the COM.

CONCLUSIONS

We have demonstrated the set-up and the functionality of an imaging spectrograph. The spectrograph consists of a highly sensitive CCD array, a grating diffraction module, a monochromatic illumination source, and a PC for control and data acquisition. By combining acquisition and data analytical techniques from traditional spectroscopy and imaging, a flexible and multi purpose system are obtained. Both spectroscopic (reflectance and fluorescence) and image data can be gathered with the system. Using the binning technique, also spectra from up to 330 local regions in a one-dimensional image of up to 22×70mm can be acquired simultaneously. The measuring techniques have been applied in the laboratory with success to three food applications: detection of wheat flour refinement, fish ageing, and porcine meat homogeneity. For the latter application combining the local spectral information with the one-dimensional image information has developed a statistical homogeneity index.

In practice, the limiting factor for use of fluorescence analysis in industry is that suitable robust instruments with optimized sampling devices are generally unavailable. The interest of industry in developing such instrumentation seems small, because mechanics and optics are just a minor part of the development costs. The new chemometric and discriminant software requires in each case the establishment of a spectral or multichannel image library with the appropriate calibrations to relevant physical and chemical analyses for establishing a source for artificial intelligence.

Operating the imaging spectrograph is a complex task, and the system is not readily adaptable for use outside a laboratory. However, the potential of the system in quality and composition studies of food products is great.

ACKNOWLEDGEMENTS

We thank Herman Zappey and Erik Mikkelsen for their help with the measurements. The Danish Academy for Technical Sciences (ATV) is thanked for the financial support to Jesper Brøndum.

REFERENCES

Andrle, R. (1994) The Angle Measure Technique: A New Method for Characterizing the Complexity of Geomorphic Lines . *Mathematical Geology* **26**, 83-97.

Bro, R. (1995) *Håndbog i Multivariabel Kalibrering (Danish)*, DSR Tryk.

Caro, R.H. (1991) Trends in Process Control and Instrumentation. *Food Technology* **45**, 62-66.

Conradsen, K. (1989) Co-occurrence Matricer som Teksturmål (Danish). *Billeder på Vej* **2**, 8-10.

Dziezak, J.D. (1986) Title Missing. *Food Technol.* **40**, 75

Esbensen, K., Hjelmen, K. and Kvaal, K. (1996) The AMT Approach in Chemometrics - First Forays. *J.of Chemometrics* **10**, 569-590.

Esbensen, K., Midtgaard, T. and Schönkopf, S. (1994) *Multivariate Analysis in Practice*, CAMO A/S, Wenneberg, Trondheim, Norway.

Giese, J. (1993) On-Line Sensors for Food Processing. *Food Technol.* **47**, 88-95.

Gunasekaran, S. (1996) Computer Vision Technology for Food Quality Assurance. *Trends in Food Science & Technology* **7**, 245-256.

Haralick, R.M., Shanmugan, K. and Dienstein, I. (1973) Textural Features for Image Classification. *IEEE Transactions on Systems, Man and Cybernetics* **3**, 610-621.

Hui, Y.H. (1996) Encyclopedia of Food Science and Technology. In: Anonymous *Encyclopedia of Food Science and Technology*, 3rd. ed. edn. pp. 2327 John Wiley and Sons, Inc., New York]

Jenks, W.G., Bublitz, C.G., Choudhury, G.S., Ma, Y.P. and Wikswo, J.P. (1996) Detection of Parasites in Fish by Superconducting Quantum Interference Device Magnometry. *J.of Food Science* **61**, 865-869.

Jensen, S.A., Munck, L. and Martens, H. (1982) Botanical constituents of wheat and wheat and wheat milling fractions. I Quantification by autofluorescence. *Cereal Chem.* **59**, 477-484.

Jensen, S.A., Reenberg, S. and Munck, L. (1989) Fluorescence analysis in fish and meat technology. In: Munck, L., (Ed.) pp. 181-192. Longman, Harlow, UK]

Mandelbrot, B.B., Passola, D.E. and Paullay, A.J. (1984) Fractal Character of Fracture Surface of Metals. *Nature* **308**, 721

Martens, H. and Næs, T. (1993) *Multivariate Calibration*, 2ed. edn. Wiley, New York.

Munck, L. (1989) *Fluorescence Analysis in Foods*, Longman, Harlow, UK.

Munck, L., Nørgaard, L., Engelsen, S., Bro, R. and Anderson, C.A. (1998) Chemometrics in food science - a demonstration of the feasibility of a highly exploratory, inductive evaluation strategy of fundamental scientific significance. *Chemometrics and Intelligent Laboratory Systems* **44**, 31-60.

NPPC (1991) Procedures to evaluate market hogs. National Pork Producers Council.

Russ, J.C. (1994) *The Image Processing Handbook,* CRC Press.

Swatland, H.J. (1995) *On-Line Evaluation of Meat*, Technomic, Lancaster, USA.

Wold, S., Esbensen, K. and Geladi, P. (1987) Principal Component Analysis. *Chemometrics and Intelligent Laboratory Systems* **2**, 37-52.